Journal of Alloys and Compounds 509 (2011) 301–310

Contents lists available at ScienceDirect

Journal of Alloys and Compounds

journal homepage: www.elsevier.com/locate/jallcom

# Effect of heating mode and sintering temperature on the consolidation of 90W–7Ni–3Fe alloys

Avijit Mondal[a], Anish Upadhyaya[b,*], Dinesh Agrawal[c]

[a] NTPC Energy Technology Research Alliance (NETRA), National Thermal Power Corporation Ltd., Greater Noida 201308, India
[b] Department of Materials Science and Engineering Indian Institute of Technology, Kanpur 208016, India
[c] The Pennsylvania State University, University Park, PA 16802, USA

ARTICLE INFO

*Article history:*
Received 6 April 2010
Received in revised form 28 August 2010
Accepted 2 September 2010
Available online 21 September 2010

*Keywords:*
Sintering
Microwave heating
Tungsten heavy alloy
Microstructure

ABSTRACT

The present study compares the sintering response of 90W–7Ni–3Fe alloys consolidated in a 2.45 GHz microwave furnace and a conventional furnace. The W–Ni–Fe compacts were sintered in a temperature range of 1200–1500 °C corresponding to solid-state as well as liquid phase sintering. The compacts were successfully sintered in a microwave furnace with about 80% reduction in the overall processing time. For both the heating modes, the W–Ni–Fe alloys exhibited significant densification prior to melt formation through solid-state sintering. The *in situ* dilatometric studies revealed that the contribution to densification from solid-state sintering is higher at lower heating rates. In comparison to conventional sintering, microwave sintered compacts showed relatively refined microstructure and higher hardness and flexural strength.



## 1. Introduction

Tungsten heavy alloys (WHAs) belong to a group of two-phase composites, based on W–Ni–Cu and W–Ni–Fe alloys. Although WHAs with Ni–Cu binder were initially developed, attention has now been focussed on heavy alloys with Ni–Fe binder because of their superior mechanical properties [1–3]. WHAs possess unique combination of properties, such as high density (16–18 g/cm$^3$), high strength (1000–1700 MPa) and high ductility (10–30%) [3], thermal conductivity and corrosion resistance. This makes them unique in many applications such as radiation shields, vibration dampers, kinetic energy penetrators and heavy-duty electrical contacts.

The highly dense W–Ni–Fe heavy alloys could be fabricated only by liquid phase sintering [4]. Dzykovich et al. [5] have quantitatively analyzed the distribution of individual elements in the tungsten grains and matrix phase in sintered W–Ni–Fe alloys. They observed that addition of Fe decreases the solubility of W in Ni and prevents the formation of an intermetallic phase. To avoid this, the matrix composition is restricted to an optimal nickel to iron ratio of 7:3 [5,6]. The sintered properties of WHAs exhibit a complex dependence on particle size, matrix composition, sintering time, temperature and atmosphere, heating/cooling rate, and post-sintering heat-treatment. Rabin et al. [7] correlated the strength and ductility of W–Ni–Fe heavy alloys with the microstructure and found that ductility of the alloys continuously decreases with increasing tungsten content and an optimal combination of strength and ductility is achieved at about 93 wt.% tungsten. Belhadjhamida and German [8] too confirmed the decrease in ductility with increasing tungsten content. However, they found that the strength of W–Ni–Fe alloy increases with an increasing tungsten content and attains a maximum at about 85 vol.% (93 wt.%) tungsten. Besides tungsten powder size and distribution, the properties of W–Ni–Fe alloys are also influenced by sintering time and temperature. Bourguignon and German [9] reported lower strength and higher ductility of 93W–4.9Ni–2.1Fe alloy liquid phase sintered at higher temperature. The strength decreased from 924 MPa to 899 MPa and the ductility increased from 14% to 27% when the sintering temperature was increased from 1465 °C to 1580 °C. This was attributed to the rate of tungsten grain growth, which results in proportionately higher fraction of matrix phase between the grains. In yet another study, Bose et al. [10] reported similar effect of temperature on strength and ductility of liquid phase sintered 90W–7Ni–3Fe system.

German et al. [11] studied the effect of sintering time on the microstructure and mechanical properties of tungsten heavy alloys. They reported that increasing sintering time obviously resulted in microstructural coarsening, which degraded the mechanical properties. During the heating process, substantial changes in terms of thermodynamics and microstructure occur with the temperature to minimize the free energy. Clearly, the changes are time and heating rate dependent. Recently, Bollina and German [12] have critically examined the effect of heating rate in conventional tech-

* Corresponding author. Tel.: +91 512 2597672; fax: +91 512 2597505.
*E-mail address:* anishu@iitk.ac.in (A. Upadhyaya).

0925-8388/$ – see front matter © 2010 Elsevier B.V. All rights reserved.
doi:10.1016/j.jallcom.2010.09.008

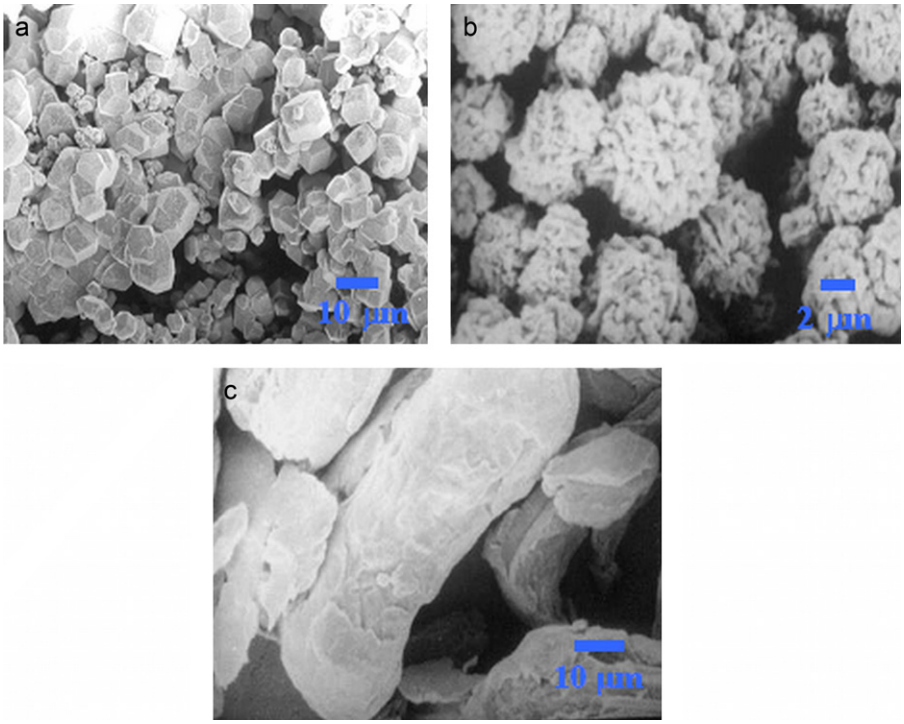


**Fig. 1.** SEM micrographs of as-received (a) W, (b) Ni, and (c) Fe powder.

nique in a range from 1 °C/min to 15 °C/min, on densification during liquid phase sintering of a range of W–Ni–Fe alloy compositions.

Conventional sintering requires long soaking time for W–Ni–Fe alloys which results in undesired grain growth and precipitation of brittle intermetallic phases. Microwave sintering of W–Ni–Fe compositions was studied by Upadhyaya et al. [13]. They investigated the sintering response of a 92.5W–7.5(Ni–Fe) alloy – with a non-optimal matrix composition – consolidated through microwaves and compared its densification, microstructure and mechanical properties with those of conventionally sintered compacts. Many studies on microwave sintering of tungsten and its alloys have been conducted earlier by several researchers [14–23]. Zhou et al. [20] investigated the effect of heating rate on the microwave sintered 90W–7Ni–3Fe heavy alloys, with the heating rate in the range from 10 °C/min to 112 °C/min. They have shown that a faster heating rate results in smaller W grain size and larger W–W contiguity. The heating rate of 80 °C/min has the best combination of the microstructure and mechanical performance. The present study evaluates the effect of heating mode and sintering temperature on the sintering of 90W–7Ni–3Fe alloys.

## 2. Experimental procedure

The as-received powders were characterized for their size, size distribution and morphology. Table 1 summarizes the characteristics of the as-received W, Ni, Fe powders used in the present study. Fig. 1 shows the scanning electron micrographs of the precursor powders. The chemically reduced tungsten powder has irregular, faceted morphology. Nickel powder, which was produced by carbonyl decomposition, resulted in a rounded morphology with spiky appearance. Iron powder was also produced by carbonyl decomposition. The alloy compositions were prepared by mixing the required proportions of each powder in a turbula mixer (model: T2C Nr 921266, supplier: Bachofen AG, Switzerland) for 60 min to ensure complete homogeneity in the resultant powder mixture. For investigating the densification response and compaction studies of various compositions, cylindrical pellets (diameter: 1.6 cm and height 0.8 cm) were pressed at 200 MPa using a uniaxial, semi-automatic hydraulic press (model: CTM 50, supplier: FIE, Ichalkaranji, India) and zinc-stearate powder as die-wall lubricant. The as-pressed green compact density varied from 54% to 56% of the theoretical density of the alloy, calculated using the inverse rule of mixtures.

To study the densification behavior, the green compacts were sintered using conventional and microwave furnace. The conventional sintering of green compacts was carried out in a $MoSi_2$-heated horizontal tubular furnace (model: OKAY 70T-7, supplier: Bysakh, Kolkata, India) at a constant heating rate of 5 °C/min. The sintering temperatures selected for the solid and liquid phase sintering of 90W–7Ni–3Fe alloys were 1200 °C, 1250 °C, 1300 °C, 1450 °C and 1500 °C, and sintering time was kept constant at 60 min. All samples were processed in flowing $H_2$ atmosphere with dew point −35 °C. Microwave sintering of the green compacts was carried out using a multi-mode cavity, 2.45 GHz, 6 kW commercial microwave furnace (model: RC/20SE, supplier: Amana Radarange). Further details of the microwave furnace and experimental arrangements have been described elsewhere [17].

The sintered density was obtained by both dimensional measurements as well as Archimedes principle. In order to take into account the influence of the initial as-pressed density, the compact sinterability was also expressed in terms of densification parameter which is calculated as follows:

$$\text{Densification parameter} = \frac{(\text{Sintered density} - \text{green density})}{(\text{Theoretical density} - \text{green density})} \quad (2)$$

To compare the densification response of various compositions, the sintered densities were normalized with respect to the theoretical density. The formulae

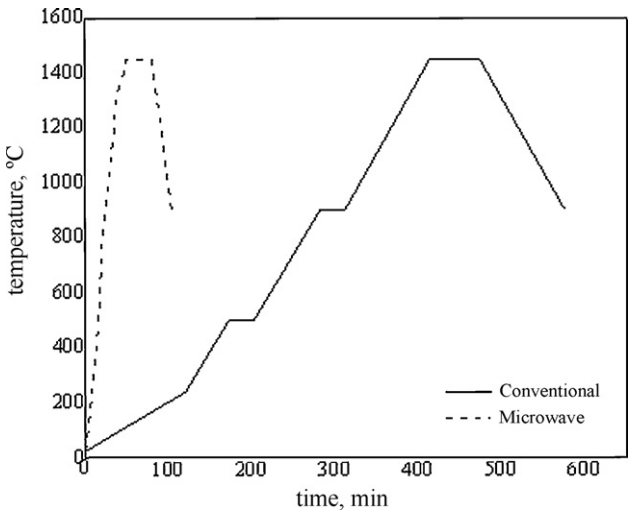


**Fig. 2.** Thermal profile of 90W–7Ni–3Fe alloy consolidated in a radiatively heated (*conventional*) and microwave furnace.

**Table 1**
Characteristics of the as-received powders used in the present study.

| Powders | W | Ni | Fe |
|---|---|---|---|
| Supplier | Kennametal Widia India Ltd. | INCO | Kennametal Widia India Ltd. |
| Processing route | Chemical reduction | Carbonyl process | Carbonyl process |
| Powder shape | Irregular | Spiky | Spherical |
| Flow rate (s/50 g) | Non-flowing | Non-flowing | 5.5 |
| (Powder size, μm) | | | |
| $D_{10}$ | 2.0 | 3.8 | 1.4 |
| $D_{50}$ | 4.2 | 11.0 | 7.0 |
| $D_{90}$ | 6.2 | 31.8 | 19.0 |
| Apparent density, g/cm$^3$ (%theoretical) | 4.8 (25%) | 2.2 (25%) | 3.1 (39%) |
| Tap density, g/cm$^3$ (%theoretical) | 6.3 (33%) | 3.1 (35%) | 3.7 (47%) |

used for calculation of axial ($\delta_A$) and radial shrinkage ($\delta_R$) of the sintered cylindrical compacts are given below:

$$\delta_A = \left(1 - \frac{h_s}{h_g}\right) \times 100\% \quad (3)$$

$$\delta_R = \left(1 - \frac{r_s}{r_g}\right) \times 100\% \quad (4)$$

where $h_g$ and $h_s$ are heights; and $r_g$ and $r_s$ are radii of the green and sintered compact, respectively.

For understanding the phenomenology of phase evolution, differential scanning calorimetry (DSC) was used. The W–Ni–Fe compacts were heated to 1500 °C at a constant rate of 10 °C/min and subsequently cooled at a controlled rate (10 °C/min) in a DSC unit (model: SDT2960, supplier: TA Instruments, New Castle, DE, USA).

For measuring *in situ* axial shrinkage and shrinkage rate during sintering dilatometry experiments were performed using a vertical push rod dilatometer in reducing atmosphere. The temperature inside the dilatometer (model: 1161V, Anter, Pittsburgh, PA, USA) was accurate to ±2 °C. It measures dimensional changes over the entire sintering cycle with precision of 1 μm. The dilatometry studies were conducted at various heating rates (2 °C/min, 5 °C/min, and 10 °C/min) and constant cooling rate of 10 °C/min. Metallographic techniques were employed on the sintered samples. The sintered samples were wet polished in a manual polisher (model: Lunn Major, supplier: Struers, Denmark) using a series of 6 μm, 3 μm and 1 μm diamond paste, followed by cloth polishing using a suspension of 0.04 μm colloidal $SiO_2$ suspension. The scanning electron micrographs of as-polished samples were obtained by a scanning electron microscope (model: Quanta, supplier: FEI, The Netherlands) in the secondary electron (SE) mode. Grain size measurement was done by line intercept method. During the measurement it was assumed that there were no sub grain boundaries inside the tungsten grain. In the present study, quantitative analysis was carried out on selected specimens using an EPMA (model: JXA-8600 SX Super-Probe, supplier: JEOL, Japan). Phase determination and phase evolution, if any were studied for all the samples using X-Ray Diffractometer (model: Rich. Seifert & Co., GmbH & Co. KG, Germany). Bulk hardness measurements were performed on polished surfaces of sintered cylindrical compacts at a load of 5 kg using Vickers hardness tester (model: V100-C1, supplier: Leco, Japan). The load was applied for 30 s. Micro hardness tester (model: 8299, supplier: Leitz, Germany) was used to evaluate the hardness of tungsten grains and the matrix phase. The loads applied on tungsten grain and matrix phase during the micro hardness measurement were 50 g and 15 g, respectively. The bulk hardness and the micro hardness values of tungsten grain and matrix phase reported for each sample were an average of five readings taken at different locations on respective phases. Transverse rupture strength (TRS) measurements of sintered samples were performed following the procedure described in MPIF Standard 41 [24].

## 3. Results and discussion

### 3.1. Heating response of W–Ni–Fe alloy

Fig. 2 compares the thermal profiles for 90W–7Ni–3Fe alloy consolidated in conventional and microwave furnaces, respectively. From the figure, it is quite evident that 90W–7Ni–3Fe samples effectively couple with the microwaves and undergo rapid heating. The overall heating rate observed in case of microwave heating was 29 °C/min. It is also interesting to note that due to the less thermal mass, the cooling rate in microwave furnace is relatively higher. Taking into consideration the slow heating rate (5 °C/min) and isothermal holds at intermittent temperatures in conventional furnace, microwave sintering results in about 80% reduction in the overall process time. These scales of the time compression are similar to those reported by Upadhyaya et al. [13] in case of 92.5W–6.4Ni–1.1Fe alloys and more recently by Zhou et al. [20] in case of 90W–7Ni–3Fe system. Fig. 3 compares the temporal power consumption in heating the 90W–7Ni–3Fe alloys. It is interesting to note that heating of the same compact in microwaves is achieved at much lower power consumption. This can be attributed to the fact that in microwaves only the sample *per se* heats up and acts as the source of heat. As a result, energy is primarily consumed in heating up the sample only. Consequently, the effective thermal mass reduction lowers the required power input. Despite such high heating rate, no micro- or macro-cracking and distortion was observed in microwave sintered samples (Fig. 4). This further underscores the efficacy of unique volumetric heating associated with microwaves.

### 3.2. Effect of heating mode and sintering temperature on densification

Fig. 5a and b show the effect of sintering temperature on the density and densification parameter of 90W–7Ni–3Fe alloy consolidated in conventional and microwave furnaces, respectively. In case of conventional sintering the compacts were sintered up to 1500 °C for 1 h. However, owing to slight distortion that was discerned in microwave sintering the compacts sintering temperature in microwave furnace was restricted to 1450 °C, 30 min. In fact, microwave sintered compacts attained nearly full (>98.5%) density at 1450 °C, 30 min. Prolonged soaking time in microwave led to distortion of the compact and therefore was not employed.

For both the heating modes, the sintered density increases with sintering temperature. Since the green density of the compacts was

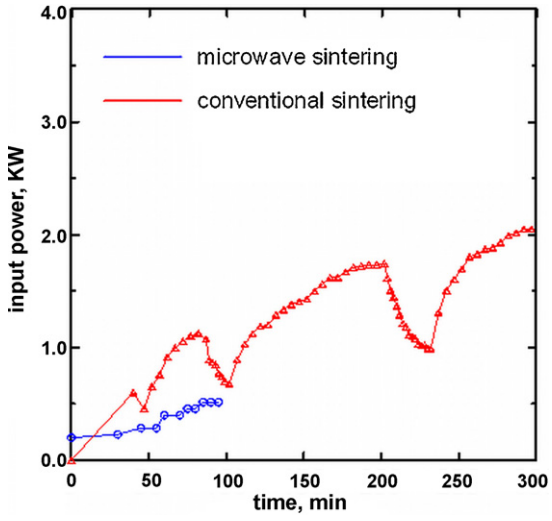


**Fig. 3.** Input power variation with time in heating of 90W–7Ni–3Fe alloy compacts in a conventional and microwave furnace.

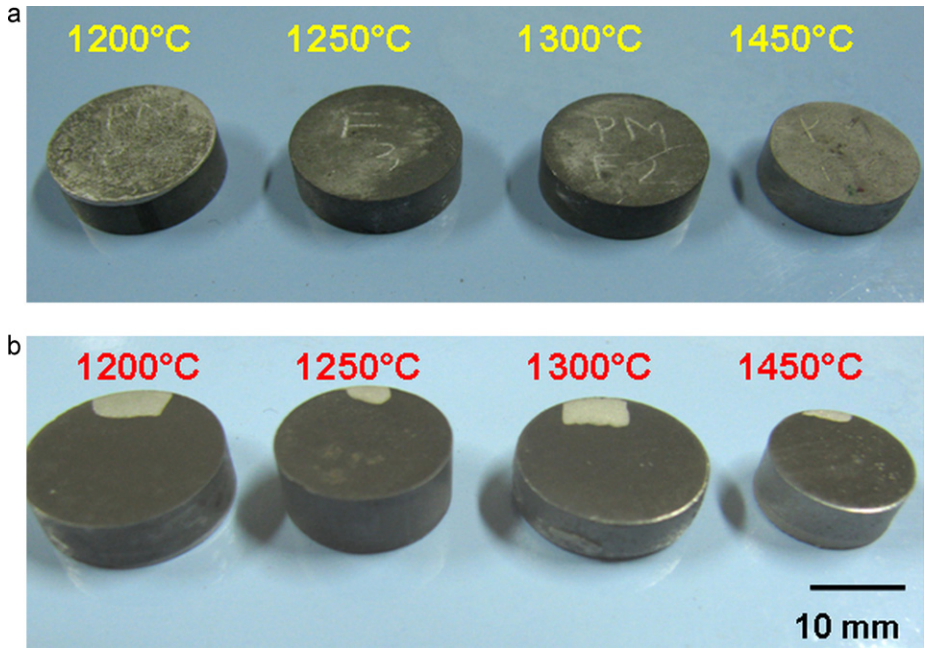


**Fig. 4.** Photographs of the 90W–7Ni–3Fe compacts sintered in (a) conventional and (b) microwave furnace at temperatures ranging between 1200 °C and 1450 °C.

maintained the same, the densification parameter follows the similar trend as sintered density. For all the sintering temperatures microwave sintering resulted in enhanced densification. In fact, microwave sintered compacts attained nearly full (>98.5%) density at 1450 °C. The increase in densification with increasing temperature can be attributed to the greater diffusivity of W in the binder. It has been reported [25,26] that the diffusivity of tungsten in nickel shows a drastic increase from $10^{-10}$ $cm^2/s$ to about $10^{-5}$ $cm^2/s$ as the temperature increases from 1200 °C to 1350 °C.

Fig. 6a and b show the variation in the radial and axial shrinkage with sintering temperature for the 90W–7Ni–3Fe alloys consolidated in conventional and microwave furnace, respectively. As evident from the figure, for both the heating modes, shrinkage of the cylindrical compacts in radial direction is invariably higher than that measured axially. The shrinkage trend correlates well with the densification results summarized in Fig. 5a. As compared to the conventional sintering, the dimensional shrinkage in both radial as well as axial direction is higher for compacts sintered in microwave furnace. Elsewhere, similar results have been reported in other systems as well by Lenel et al. [27] and El-Shanshoury and Nazmy [28]. The anisotropy in the shrinkage has been attributed to the asymmetry of the pore shape and its curvature that results due to the compaction of the powders. As a result the radial direction undergoes more shrinkage due to pore rounding. From Fig. 6, it can also be inferred that the above trend (i.e. more radial shrinkage) is more accentuated in case of microwave sintered compacts. While the exact reason for this is not clear, however, based on the modeling results [22] and literature report [29], it is hypothesized that the curvature difference of the pores in the cylindrical compacts may have resulted in differential microwave coupling, which, in turn, may result in asymmetric dimensional change during heating.

To understand phenomenology of densification during sintering, it is important to first evaluate the phase changes that occur in the premixed W–Ni–Fe powder compacts during thermal cycling. To isolate the influence of tungsten addition on the associated phase changes, DSC analysis was conducted separately for 70Ni–30Fe and 90W–7Ni–3Fe system. The corresponding DSC curves are presented in Figs. 7 and 8, respectively. For the 90W–7Ni–3Fe compact, two sequential endothermic peaks are formed at 1419 °C and 1441 °C during heating (Fig. 7a), and the corresponding exother-

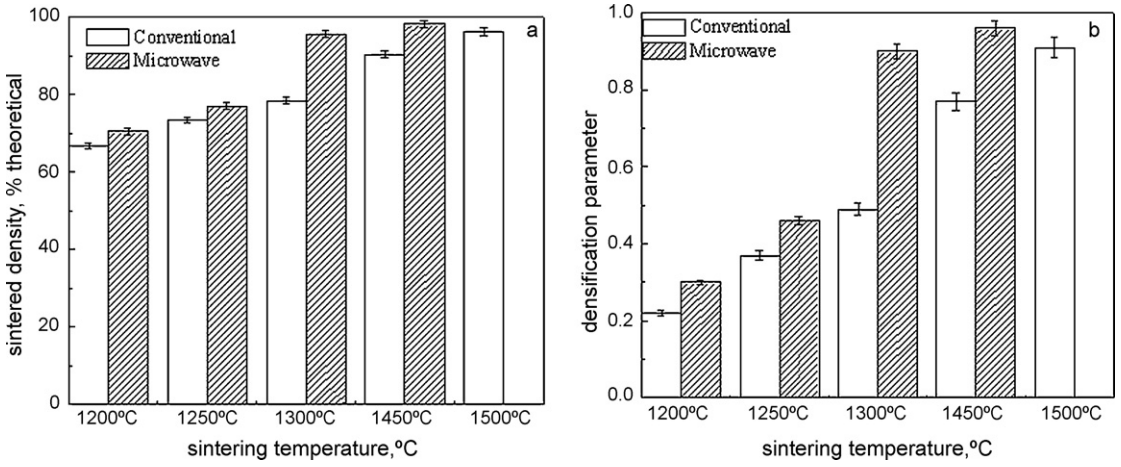


**Fig. 5.** Effect of sintering temperature on the (a) density and (b) densification parameter of 90W–7Ni–3Fe alloys consolidated in conventional and microwave furnace.

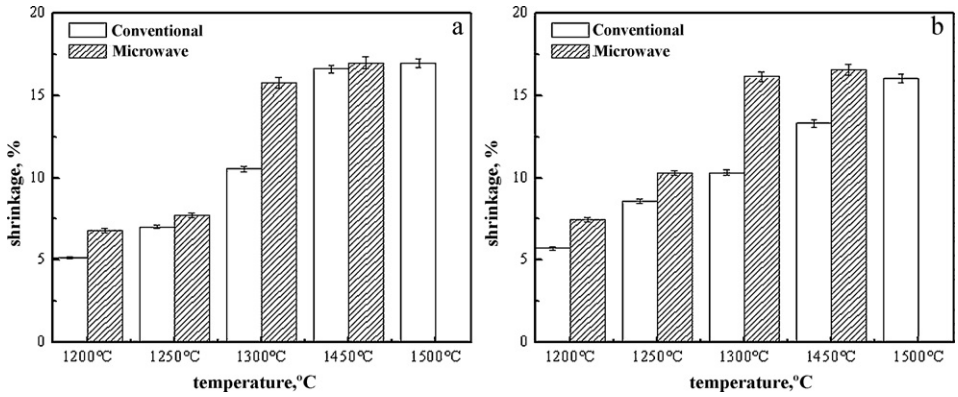


**Fig. 6.** Effect of sintering temperature and heating mode on the (a) axial and (b) radial shrinkage of 90W–7Ni–Fe alloys.

mic peak upon cooling occurs at 1436 °C and 1445 °C, respectively (Fig. 7b). According to the Fe–Ni phase diagram [30], iron and nickel are mutually soluble over a wide temperature range. The 30:70 ($\gamma$ Fe, Ni) alloy melts congruently at 1445 °C. The endothermic peak at 1441 °C is related to the melting temperature of Ni–Fe alloys. The depression in the solidification temperature under non-equilibrium processing condition is well known [31]. Compared with 7Ni–3Fe, the 90W–7Ni–3Fe compact exhibits a much similar temperature range for liquid-phase formation and solidification. During heating (Fig. 8a), the endothermic peak at 1477 °C represents the melting of the Ni–Fe matrix. In accordance, the exothermic peak appears at 1471 °C (Fig. 8b) corresponds to the solidification of the binder melt. It is evident that the melting temperature of the Ni–Fe matrix is well above the melting point of elemental nickel and does not significantly change with the *in situ* alloying among elemental Ni, Fe, and W powders. This agrees well with the equilibrium conditions in Fe–Ni and Fe–Ni–W phase diagrams [30,32]. According to the Fe–Ni phase diagram [30], iron and nickel are mutually soluble over a wide temperature range. The 30:70 ($\gamma$ Fe, Ni) alloy melts congruently at 1445 °C. In the Fe–Ni–W ternary alloys phase diagrams [32], ($\gamma$ Fe, Ni) also acts as one of the main phases between 800 °C and 1500 °C, and the eutectic Ni–Fe–W liquid phase forms at 1465 °C. Besides liquid-phase formation, the sintering process in the W–Ni–Fe alloy system may also involve some other phase changes, most of which relate to the forma-

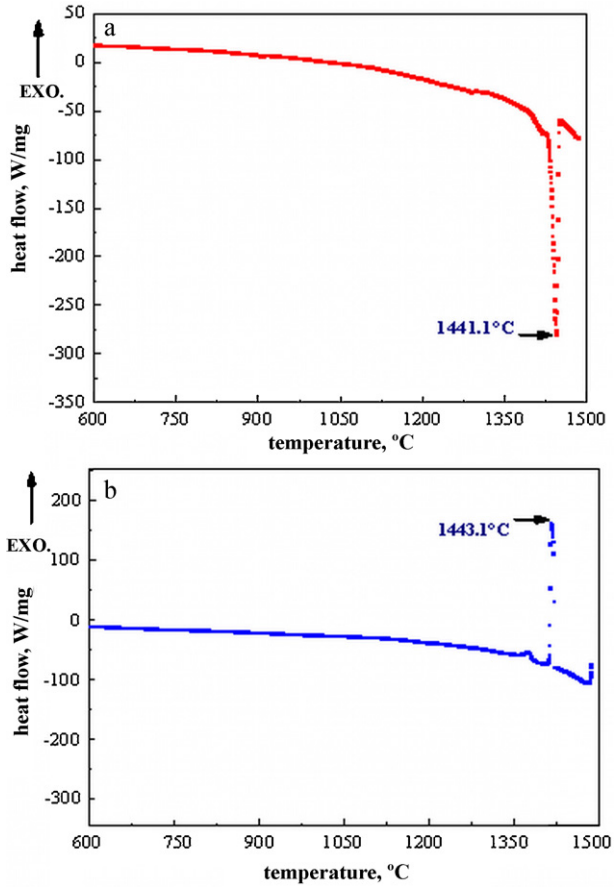


**Fig. 7.** DSC analysis of 70Ni–30Fe alloy powder during (a) heating and (b) cooling at a constant rate of 10 °C/min. The powders were heated up to 1500 °C in argon.

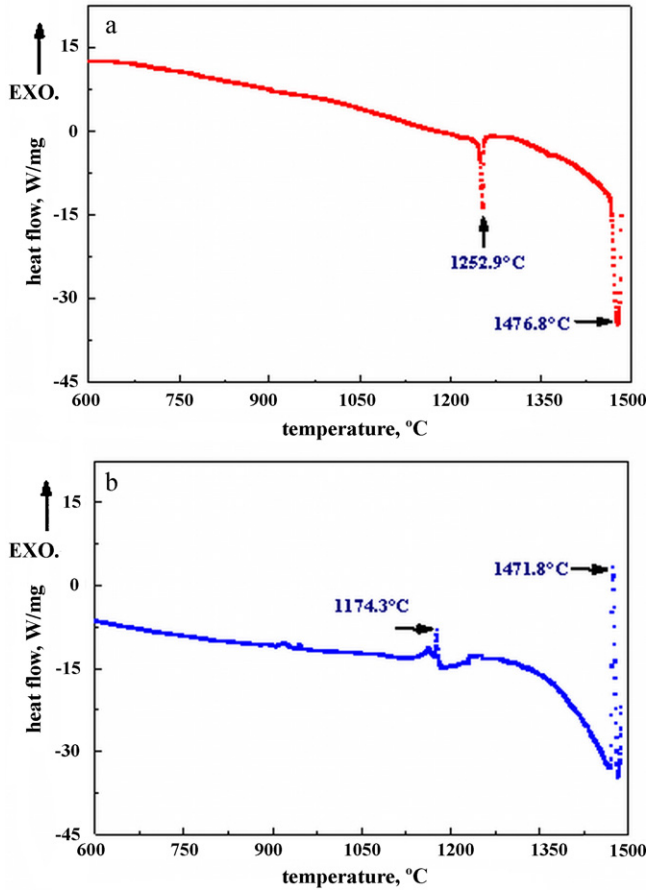


**Fig. 8.** DSC analysis of 90–7Ni–3Fe powder mixture during (a) heating and (b) cooling at a constant rate of 10 °C/min. The powders were heated up to 1500 °C in argon.

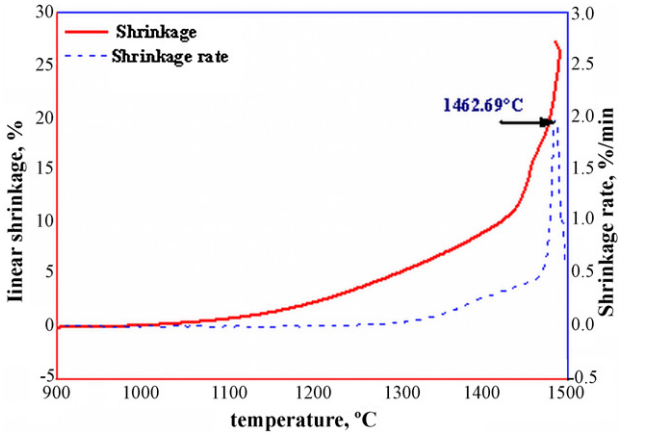


**Fig. 9.** Dilatometric shrinkage and shrinkage rate curve of 90W–7Ni–3Fe compacts heated up to 1500 °C at a constant heating rate of 10 °C/min.

tion of intermetallics [33,34]. As evident in Fig. 8, an endothermic peak forms at 1253 °C for the 90W–7Ni–3Fe compact during heating (Fig. 6a), and an exothermic peak appears at 1174 °C upon its cooling (Fig. 8b). These two peaks are very likely resulted from the transformation of $Fe_7W_6$, which is the sole intermetallic phase in the Fe–Ni–W alloy system above 1150 °C [32]. The results from the present study correspond well with those reported elsewhere [12,35,36]. Unlike the previous reports [33,34], the alloy used in the present study had a stoichiometric binder composition (Ni:Fe 7:3), hence, formation of the intermetallic is not expected. However, as the composition in the present study was prepared by powder mixing, it is likely that this may have caused some local inhomogeneity that may have resulted in formation of small amounts of intermetallic phases which sensitive equipment such as DSC can readily detect. To ensure good homogeneity, it would be interesting to conduct further studies using prealloyed Ni–Fe powders instead of the premixed ones.

From the DSC curves, it can be inferred that out of the five temperatures selected for conventional sintering, lower temperatures (1200 °C, 1250 °C and 1300 °C) correspond to solid-state sintering, and the higher ones (1450 °C and 1500 °C) to liquid phase sintering. It is well known that due to faster diffusion rate and capillary-induced stresses the densification kinetics is higher during liquid phase sintered compacts [37]. The densification response of the alloys in the present study (Fig. 5b) confirms that they are in accordance with this. Another factor that contributes to densification during liquid phase sintering is that the newly formed wetting melt spreads to fill the small pores and preferentially penetrates the grain boundaries [37,38]. Since tungsten has substantial solubility into the Ni–Fe matrix, hence the melt tends to dissolve the interparticle necks and spreads out [39], this results in the decrease of the solid–liquid interfacial energy below that of the equilibrium value [40] and further contributes to densification in the initial period just after melt formation.

To obtain a better insight about the densification response of the 90W–7Ni–3Fe compacts, Fig. 9 plots the shrinkage and shrinkage rate data of the alloy at various temperatures during heating at a rate of 10 °C/min in a dilatometer. The compact did not show any significant dimensional change till about 1000 °C. From the figure, it is quite evident that up to 900 °C the compact does not undergo any significant shrinkage. Subsequently, a substantial portion of the densification (10% linear shrinkage) occurs prior to the melt formation. This is in agreement with the similar observations reported by other researchers [41–43]. From the shrinkage rate curve (Fig. 9) it is evident that there is a sudden increase in the densification at 1463 °C. Taking into account the error in temperature measurement and the differences in the atmosphere used, this closely corresponds with the melt formation temperature of this alloy determined using DSC (Fig. 8) and reported by others [12,35,36]. The enhanced densification at the onset of melting is due to the capillary-induced arrangement. In addition, melt formation also results in enhanced tungsten solubility. The tungsten is

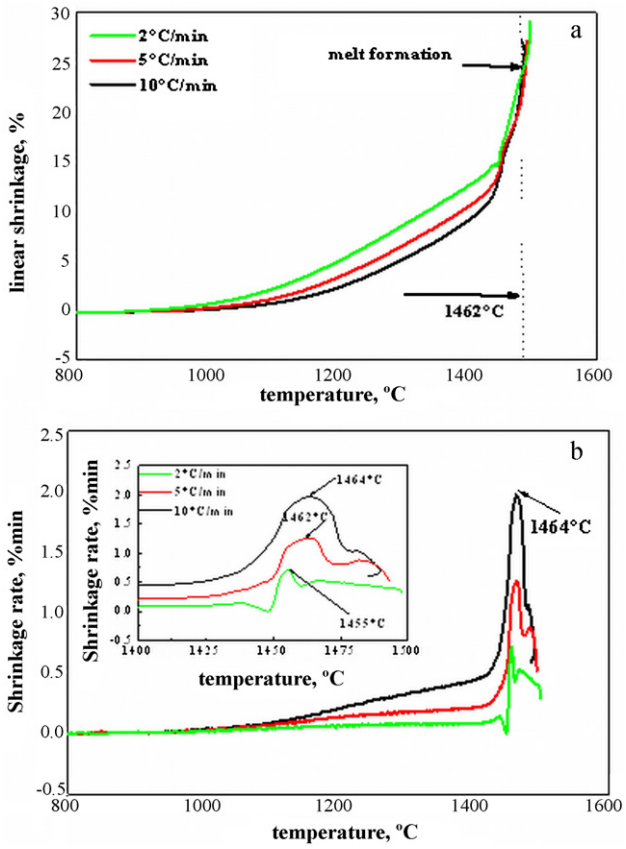


**Fig. 10.** Dilatometric plots showing the effect of heating rate on the (a) linear shrinkage and (b) shrinkage rate of 90W–7Ni–3Fe alloy heated up to 1500 °C in reducing atmosphere.

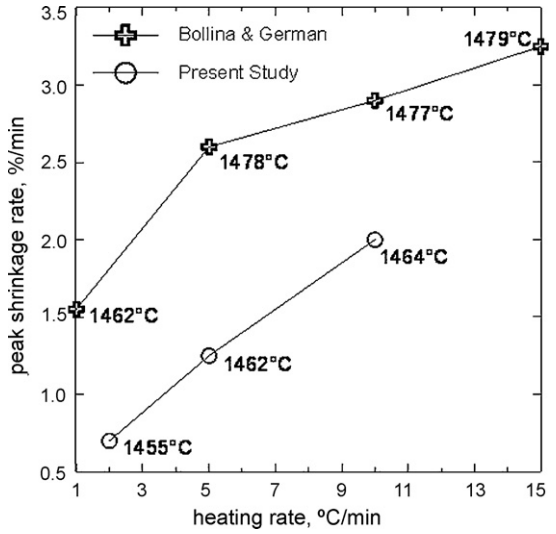


**Fig. 11.** The peak shrinkage rate of 90W–7Ni–3Fe alloy at the onset of liquid formation temperature plotted as a function of heating rate. The temperature at which the peak shrinkage occurs is also indicated on the plot. The data from Bollina and German [12] on 88W–Ni–Fe (7:3) have also been superimposed for the sake of comparison.

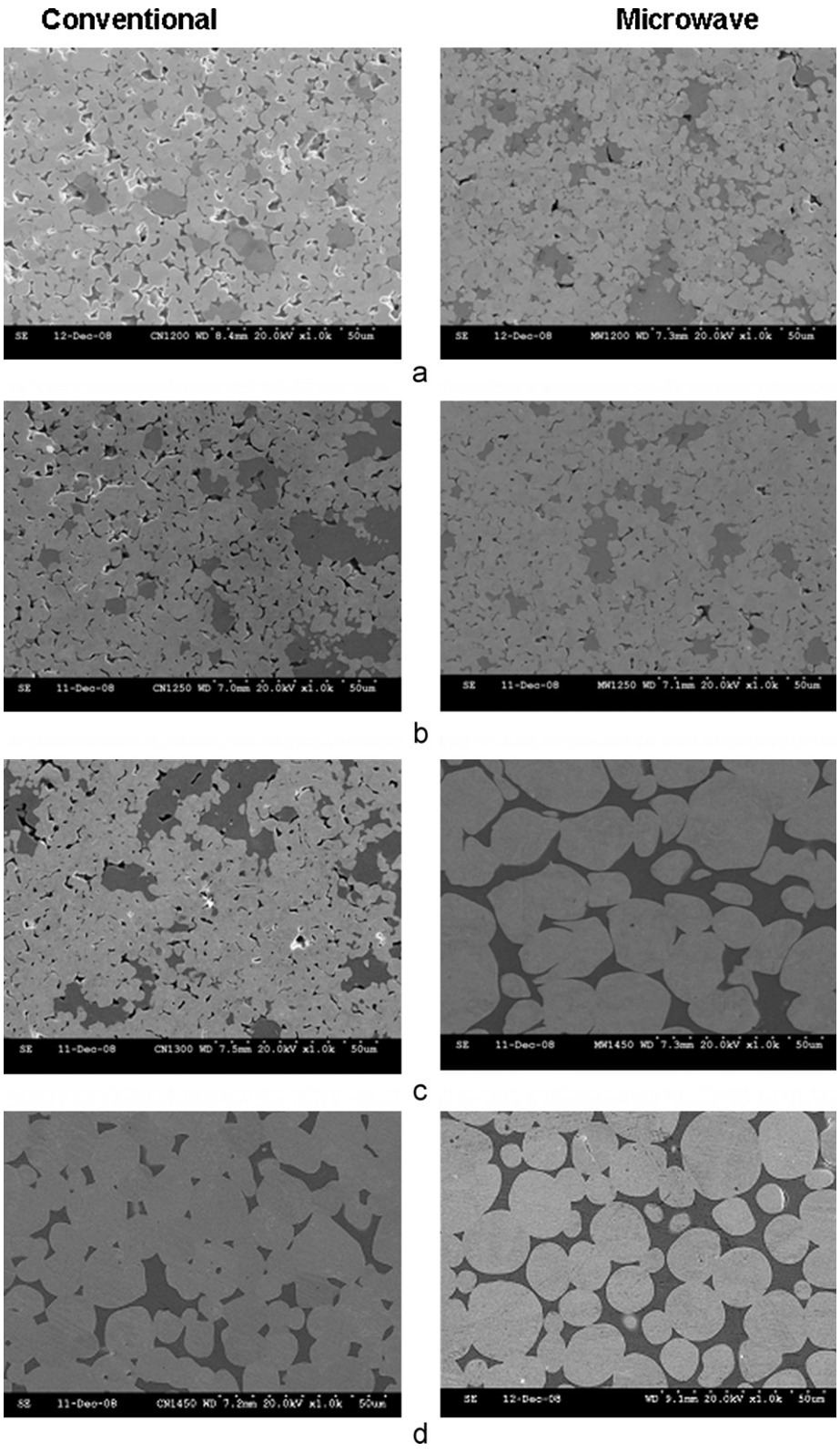


**Fig. 12.** SEM micrographs of 90W–7Ni–3Fe compacts sintered in a conventional furnace (*left*) and microwave furnace (*right*) at (a) 1200 °C, (b) 1250 °C, 1300 °C and (b) 1450 °C, respectively.

preferentially dissolved from the interparticle necks and/or sharp curvatures. This results in disruption of the solid-state sintered W–W bonds and causes grain shape accommodation. Both results in activating densification kinetics and accounts for the greater shrinkage rates observed in Fig. 9.

In the above section, dilatometric investigation aided in understanding the influence of temperature on the phenomenology of densification. Besides temperature, heating rate is also an important parameter that influences the densification since it influences not only the diffusivity but also alters the phase transforma-

tion temperature. Unfortunately, owing to the limitation of the dilatometer used in the present investigation, the fast heating rates obtained in microwave heating could not be achieved. Hence, to evaluate the influence of heating rate on the sinterability, the 90W–7Ni–3Fe compacts were heated up to 1500 °C at three heating rates, namely 2 °C/min, 5 °C/min and 10 °C/min in a dilatometer. The corresponding shrinkage and shrinkage rate variation at the three heating rates are summarized in Fig. 10a and b, respectively. It is interesting to note that the contribution to densification from solid-state sintering is higher at lower heating rates (Fig. 10a). In the temperature range corresponding to onset of melting, the effect of heating rate is better reflected in the shrinkage rate plot (Fig. 10b) since it is more sensitive to small changes in temperature. Interestingly, the contribution of liquid phase sintering to densification is higher for alloys sintered at higher heating rate. Similar effect of heating rate on the shrinkage and shrinkage rate were observed by Bollina and German [12] in 88W–Ni–Fe alloy (Ni/Fe ratio 7:3). The shrinkage rate results near binder melting temperature (plotted as inset to Fig. 10b) reveals that both the shrinkage rate and matrix melting temperature shift to higher values as the heating rate increases [Fig. 10b (inset)]. Fig. 11 shows the peak temperature corresponding to the maximum shrinkage rate in the present alloy at various heating rates and along with the results from Bollina and German [12] in a similar alloy system.

At any temperature the shrinkage rate is lower for a slower heating rate. The point of maximum shrinkage rate indicates the dissolution of solid-solid bonds by liquid phase and densification due to rearrangement. If the solid-state densification is suppressed, then melt formation significantly contributes to densification of the compact. The shrinkage at any given temperature is higher for the slower heating rate of 2 °C/ min, since the slower heating rate gives more time for solid-state diffusion prior to liquid formation. As the compact becomes more dense prior to reaching the liquid formation temperature, hence the contribution from liquid phase sintering proportionately decreases at slower heating rates [44]. By extending this argument it is hypothesized that during microwave sintering the major contribution to densification stems from liquid phase sintering. It is envisaged that the fast heating rates achieved through microwaves restrict the W–W bond formation prior to melting and thereby making the contribution to densification from rearrangement more effective. Elsewhere too, researchers [44–46] have proposed that slow heating rates are detrimental to rearrangement.

### 3.3. Microstructural evolution during conventional and microwave sintering

Fig. 12a–d compare the effect of heating mode on the microstructure of the 90W–7Ni–3Fe compacts sintered at 1200 °C, 1250 °C, 1300 °C, and 1450 °C, respectively. At 1500 °C, the W–Ni–Fe compacts were only conventionally sintered and the corresponding microstructure is presented in Fig. 13. As expected, for both conventional as well microwave heating, higher sintering temperatures, result in reduced porosity, more homogenous distribution of the binder phase and coarser tungsten grains. For compacts sintered at 1200 °C and 1250 °C, the microstructures are typical of those expected from solid-state sintering. In case of conventional sintering, the compacts sintered at 1300 °C, again corresponds to solid-state sintering. In comparison, while the microstructure of compacts conventionally sintered at 1450 °C exhibit significant grain coarsening, the tungsten grains still have irregular shape which underscores solid-state sintering. Further increase in the sintering temperature to 1500 °C results in a typical liquid phase sintered microstructure with well-rounded and less contiguous tungsten grains interspersed in a Ni–Fe matrix (Fig. 13). These results when looked in isolation are as per

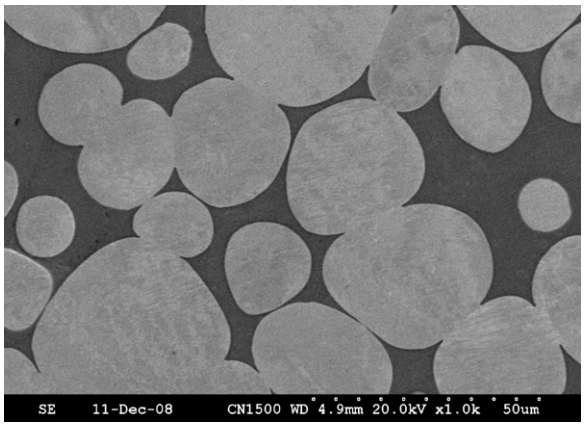


**Fig. 13.** Representative microstructure of 90W–7Ni–3Fe alloy liquid phase sintered at 1500 °C in a conventional furnace.

expected and correlate well with the DSC (Fig. 7) and dilatometric (Fig. 8) observations. However, the corresponding microstructures of 90W–7Ni–3Fe alloys microwave sintered at 1300 °C and 1450 °C (Fig. 12c and d) are very intriguing. The samples microwave sintered at these temperatures show significantly coarse tungsten grains and the microstructure is similar to that expected of a typically liquid phase sintered W–Ni–Fe alloy! In view of the fact that the matrix melting temperature in these alloys is elevated as the heating rate increases (Fig. 11), this is even more perplexing. This finding was validated by several repeated experiments. These results are similar to those reported in 90W–7Ni–3Cu system [19] and need to be more critically investigated.

One of the probable cause of this observation can be attributed to the inherent problem in accurately measuring temperature during microwave sintering. The temperature measurement for the present study was done by optical pyrometer. To address this inherent limitation, temperature was also measured using a more accurate emmissivity-based infra-red pyrometer, wherein, the emmissivity at various elevated temperatures was calibrated (for the same composition compacts) in a conventional furnace. Even in this, same results were obtained. One of the probable reasons for this observation is also the critique that the pyrometer based temperature measurements are an average of the surface temperature only. It may be likely that – for multi-component system, such as W–Ni–Fe alloys – the temperature in the interior of the sample may be slightly higher. However, no gradient in the microstructure was obtained in the sintered samples. One of the likely explanations for such an observation therefore could be the differential coupling of the constituents with microwave thereby leading to anisothermal heating effect that has been reported to cause rapid diffusion rates and onset of liquid phase sintering at lower temperatures [47,48]. Besides microstructural coarsening, as a consequence of this enhanced diffusion, the densification is expected to be high, which is indeed the case (Fig. 5). This is further confirmed by the EPMA results summarizing the effect of heating mode and sintering temperature on the composition of the matrix phase. Note that irrespective of the temperature, the amount of dissolved tungsten in microwave sintered alloy is higher than those consolidated conventionally (Table 2).

Fig. 14a and b compare the XRD patterns of the samples sintered at various temperatures in conventional and microwave furnace, respectively. As discussed earlier, the choice of a stoichiometric binder ratio (7:3) obviates intermetallic formation in any of the sintered compact. The microwave sintered 90W–7Ni–3Fe alloys are characterized by a change in the peak intensity and absence of some of the matrix diffraction peaks. Such observations have also been noticed in other systems as well and have been attributed to the

**Table 2**
Effect of heating mode and sintering temperature on the composition of the matrix phase in 90W–7Ni–3Fe alloys.

| Temperature, °C | Heating mode | Elemental content, wt. % | | |
|---|---|---|---|---|
| | | W | Ni | Fe |
| 1200 °C | Conventional | 8.11 ± 5.85 | 24.65 ± 17.85 | 67.48 ± 24.34 |
| | Microwave | 19.14 ± 10.9 | 45.24 ± 12.41 | 35.63 ± 24.62 |
| 1250 °C | Conventional | 27.38 ± 5.8 | 57.67 ± 0.81 | 11.21 ± 6.35 |
| | Microwave | 30.23 ± 4.58 | 58.45 ± 0.38 | 10.18 ± 5.17 |
| 1300 °C | Conventional | 21.04 ± 3.65 | 53.96 ± 4.00 | 23.19 ± 7.48 |
| | Microwave | 28.43 ± 0.5 | 51.07 ± 0.12 | 20.65 ± 0.41 |
| 1450 °C | Conventional | 23.19 ± 1.05 | 52.63 ± 0.58 | 21.3 ± 0.34 |
| | Microwave | 25.62 ± 0.66 | 51.48 ± 0.28 | 21.7 ± 0.27 |
| 1500 °C | Conventional | 22.96 ± 1.71 | 52.5 ± 0.76 | 21.77 ± 0.34 |
| | Microwave | – | – | – |

**Table 3**
Effect of heating mode and sintering temperature on the average grain size, transverse rupture strength (TRS) and hardness (bulk and micro) of the 90W–7Ni–3Fe compacts.

| Sintering temperature , °C | Heating mode | Grain size, μm | Hardness HV5 | Vickers microhardness | | TRS MPa |
|---|---|---|---|---|---|---|
| | | | | *W*HV0.05 | Matrix$HV0.0_{15}$ | |
| 1300 | CON | – | 161 ± 27 | – | – | 212 |
| | MW | 17 ± 7 | 325 ± 15 | – | – | 751 |
| 1450 | CON | 18 ± 11 | 289 ± 23 | – | – | 782 |
| | MW | 20 ± 7 | 352 ± 11 | 475 ± 15 | 403 ± 14 | 1800 ± 11 |
| 1500 | CON | 26 ± 14 | 329 ± 17 | 454 ± 8 | 402 ± 14 | 1796 ± 19 |

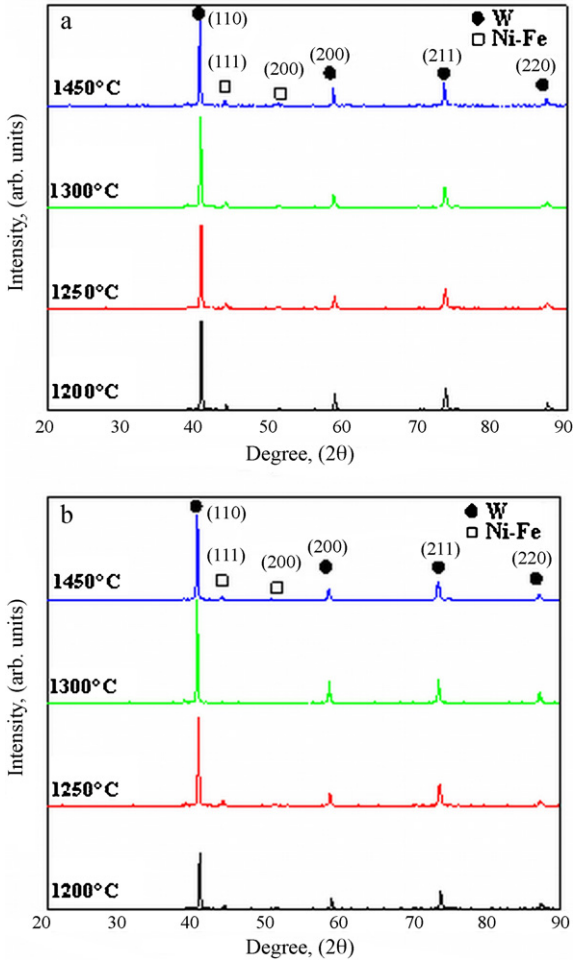


**Fig. 14.** XRD plots showing the effect of sintering temperature on the phase evolution in 90W–7Ni–3Fe alloy sintered in (a) conventional and (b) microwave furnace.

creation of defects upon interaction with the microwaves [48,49]. The presence of such defects and their nature needs to be investigated further through transmission electron microscopy (TEM) and orientation imaging microscopy (OIM/EBSD) techniques.

### 3.4. Mechanical properties of sintered W–Ni–Fe alloys

Table 3 summarizes the effect of heating mode and sintering temperature on the average grain size, bulk and micro-hardness and the flexural strength of the 90W–7Ni–3Fe alloys. Owing to the fine and contiguous microstructure, it is rather difficult to accurately measure the tungsten grain size in solid-state sintered compacts. For conventional sintering, the grain size measurements were performed for samples sintered at 1450 °C and 1500 °C. In case of microwave sintering, the grain sizes were quantified for compacts sintered at 1300 °C and 1450 °C. Note that as compared to conventionally liquid phase sintered alloys, the grain size was lower for compacts consolidated in microwave furnace. This, along with a higher sintered density, resulted in significantly higher hardness and the bend strength in microwave sintered alloys. The hardness values are similar or better than those reported previously [50,51]. The higher transverse rupture strength in microwave sintered samples can be attributed with the spheroidal tungsten grains which are less contiguous and hence provide higher mean free path for crack propagation [52–54]. It is well-recognized that the mechanical properties of the as-sintered W–Ni–Fe alloys can be further improved by heat-treatment [55,56]. In view of the high tungsten solubility in the matrix, anomalous microstructural and phase evolution during sintering, a future extension of the present set of study could be to evaluate critically the detailed DSC analysis of the composition and also the effect of thermo-mechanical treatment on the mechanical properties of microwave sintered tungsten heavy alloys.

## 4. Conclusions

In this study, 90W–7Ni–3Fe alloys were successfully sintered both through solid-state as well as liquid phase sintering

in microwave furnace. As compared to conventional sintering, microwave sintering resulted in about 80% reduction in the overall processing time. To evaluate the influence of heating rate on the sinterability, the 90W–7Ni–3Fe compacts were heated up to 1500 °C at three heating rates, namely 2 °C/min, 5 °C/min and 10 °C/min in a dilatometer. The W–Ni–Fe alloys exhibit significant densification prior to melt formation through solid-state sintering. The *in situ* dilatometric studies reveal that the contribution to densification from solid-state sintering is higher at lower heating rates. By corollary, the contribution of liquid phase sintering to densification is higher for alloys sintered at higher heating rate. It is also interesting to note that microwave sintered compacts had a well-developed liquid phase sintered structure at about 50 °C lower temperature as compared to conventional sintering. Accordingly, microwave sintered compacts had about 23% lower tungsten grain size and 22% improvement in the bulk hardness (352 VHN). As compared to 90W–7Ni–3Fe alloys sintered at 1450 °C in a conventional furnace, microwave sintering led to significant (∼130%) improvement in the transverse rupture strength from 782 MPa to 1800 MPa.

## Acknowledgement

This collaborative research was done as a part of the Center for Development of Metal-Ceramic Composites through Microwave Processing which was funded by the Indo-US Science and Technology Forum (IUSSTF), New Delhi.

## References

[1] A. Upadhyaya, Trans. Indian Inst. Met. 55 (2002) 51–69.
[2] E. Lassner, W.D. Schubert, Tungst: Properties, Chemistry, Technology of the Elements, Alloys, Chemical Compounds, Kluwer Academic/Plenum Publishers, New York, NY, USA, 1999.
[3] V. Srikanth, G.S. Upadhyaya, Int. J. Refract. Hard Met. 5 (1986) 49–54.
[4] R.M. German, Liquid Phase Sintering, Plenum Press, NY, 1985.
[5] I.Y. Dzykovich, R.V. Makarova, O.K. Teodorovich, I.N. Frantsevich, Sov. Powder Metall. Met. Ceram. 4 (1965) 655–660.
[6] S.G. Caldwell, in: A. Bose, R.J. Dowding (Eds.), Tungsten and Tungsten Alloys—1992, Metal Powder Industries Federation, Princeton, NJ, 1992, pp. 89–96.
[7] B.H. Rabin, A. Bose, R.M. German, Int. J. Powder Metall. 25 (1989) 21–27.
[8] A. Belhadjhamida, R.M. German, in: E.S. Crowson, Chen (Eds.), Tungsten and Tungsten Alloys—Recent Advances, The Minerals, Metals & Materials Society, Warrendale, PA, USA, 1991, pp. 3–19.
[9] L.L. Bourguignon, R.M. German, Int. J. Powder Metall. 24 (1988) 115–121.
[10] A. Bose, D. Sims, R.M. German, Metall. Trans. A 19 (1988) 487–494.
[11] R.M. German, A. Bose, S.S. Mani, Metall. Trans. A 23 (1992) 211–219.
[12] R. Bollina, R.M. German, Int. J. Refract. Met. Hard Mater. 22 (2004) 117–127.
[13] A. Upadhyaya, S.K. Tiwari, P. Mishra, Scripta Mater. 56 (2007) 5–8.
[14] M. Jain, G. Skandan, K. Martin, K. Cho, B. Klotz, R. Dowding, D. Kapoor, D. Agarwal, J. Chang, Int. J. Powder Metall. 42 (2006) 53–57.
[15] M. Jain, G. Skandan, K. Martin, K. Cho, B. Klotz, R. Dowding, D. Kapoor, D. Agarwal, J. Chang, Int. J. Powder Metall. 42 (2006) 45–50.
[16] G. Prabhu, A. Charkraborty, B. Sarma, Int. J. Refract. Met. Hard Mater. 27 (2009) 545–548.
[17] A. Mondal, A. Upadhyaya, D. Agrawal, J. Microwave Power Electromagn. Energy JMPEE 43 (2009) 11–16.
[18] S.D. Luo, J.H. Yi, Y.L. Guo, Y.D. Peng, L.Y. Li, J.M. Ran, J. Alloys Compd. 473 (2009) L5–L9.
[19] A. Mondal, A. Upadhyaya, D. Agrawal, Mater. Sci. Eng. A 527 (2010) 6870–6878.
[20] C. Zhou, J. Yi, S. Luo, Y. Peng, L. Li, G. Chen, J. Alloys Compd. 482 (2009) L6–L8.
[21] A. Mondal, D. Agrawal, A. Upadhyaya, J. Microwave Power Electromag. Energy JMPEE, 44, in press.
[22] A. Mondal, Modeling of Microwave Heating of Particulate Metals and its Application in Sintering of Tungsten-Based Alloys, Ph.D. Thesis, The Indian Institute of Technology, Kanpur, 2010.
[23] D. Agrawal, J. Cheng, M. Jain, G. Skandan, R. Dowding, K. Cho, B. Klotz, D. Kapoor, Eighth Int. Conf. Sci. Hard Mater., 2004, pp. 143–144.
[24] MPIF Standard 41, Standard Test Methods for Metal Powders and Powder Metallurgy Products, MPIF, Princeton, New Jersey, USA, 2002, pp. 55–57.
[25] G.E. Murch, C.M. Bruff, Diffus. Solid Met. Alloys 26 (1990) 279–371.
[26] J.P. Leonard, T.J. Renk, M.O. Thompson, M.J. Aziz, Metall. Mater. Trans. A 35 (2004) 2803–2807.
[27] F.V. Lenel, H.H. Hausner, E. Hayashi, G.S. Ansell, Powder Metall. 8 (1961) 25–36.
[28] I.A. El-Shashoury, M.Y. Nazmy, Powder Metall. 11 (1968) 63–72.
[29] M. Wllert-Porada, Microwave: Theory and Applications in Materials Processing IV, 1998, pp. 158–164.
[30] J.I. Goldstein, Alloy Phase Diagram, ASM Metals Reference Book, American Society for Metals, Metals Park, OH, 1981.
[31] D.M. Stefanescu, Science and Engineering of Casting Solidification, 2nd ed., Springer, New York, NY, USA, 2009, pp. 1–20.
[32] P. Villars, A. Prince, H. Okamoto, Handbook of Ternary Alloy Phase Diagrams, ASM International, Materials Park, OH, 1997.
[33] B.C. Muddle, Metall. Trans. A 15 (1984) 1089–1098.
[34] J.B. Posthill, D.V. Edmonds, Metall. Trans. A 17 (1986) 1921–1934.
[35] S.S. Mani, R.M. German, Advances in Powder Metallurgy, vol. 1, Metal Powder Industries Federation, Princeton, NJ, 1990, pp. 453–467.
[36] Y. Wu, R.M. German, B. Marx, P. Suri, R. Bollina, J. Mater. Sci. 38 (2003) 2271–2281.
[37] V.L. Yupko, R.V. Minakova, O.P. Kolchin, L.S. Vodopyanova, N.I. Monastyreva, V.L. Voitenko, Sov. Powder Metall. Met. Ceram. 22 (1983) 44–47.
[38] R.M. German, P. Suri, S.J. Park, J. Mater. Sci. 44 (2009) 1–39.
[39] L. Ekbom, A. Eliasson, Processing of Powder Metallurgy World Congress PM'94, vol. II, European Powder Metallurgy Association, Shrewsbury, UK, 1994, pp. 1565–1572.
[40] I.A. Aksay, C.I. Hoge, J.A. Pask, J. Phys. Chem. 78 (1974) 1178–1183.
[41] A. Upadhyaya, J. Mater. Chem. Phys. 67 (2001) 101–110.
[42] W.E. Gurwell, in: A. Bose, R.J. Dowding (Eds.), Tungsten and Refractory Metals, vol. 2, Metal Powder Industries Federation, Princeton, NJ, 1994, pp. 65–75.
[43] F. Akhtar, Int. J. Ref. Met. Hard Mater. 26 (2008) 145–151.
[44] R.M. German, S. Farooq, in: S. Sōmiya, M. Shimada, M. Yoshimura, R. Watanabe (Eds.), Sintering'87, vol. 1, Elsevier Science Publishing Co. Inc., New York, NY, 1988, pp. 459–464.
[45] G.J. Shu, K.S. Hwang, Mater. Trans. 46 (2005) 298–302.
[46] B.D. Storozh, P.S. Kislyi, Powder Metall. Met. Ceram. 13 (2005) 712–716.
[47] R.D. Peelamedu, R. Roy, D. Agrawal, Mater. Res. Bull. 36 (2001) 2723–2739.
[48] R. Roy, Y. Fang, J. Cheng, D.K. Agrawal, J. Ceram. Am. Soc. 88 (2005) 1640–1642.
[49] R. Peelamedu, R. Roy, L. Hurtt, D. Agrawal, A.W. Fliflet, D. Lewis III, R.W. Bruce, Mater. Chem. Phys. 88 (2004) 119–129.
[50] V. Srikanth, G.S. Upadhyaya, J. Mater. Sci. Lett. 7 (1988) 195–197.
[51] M. Debata, A. Upadhyaya, J. Mater. Sci. 39 (2004) 2539–2541.
[52] G.S. Upadhyaya, V. Srikanth, Modern Developments in Powder Metallurgy, vol. 17, Metal Powder Industries Federation, Princeton, NJ, 1985, pp. 51–75.
[53] I.S. Humail, F. Akhtar, S.J. Askari, M. Tufail, X. Qu, Int. J. Refract. Met. Hard Mater. 25 (2007) 380–385.
[54] S.H. Islam, X. Qu, S.J. Askari, M. Tufail, X. He, Rare Met. 26 (2007) 200–204.
[55] S.G. Caldwell, Int. J. Powder Metall. 39 (2003) 43–51.
[56] W.H. Baek, M.H. Hong, E.P. Kim, J.W. Noh, S. Lee, H.S. Song, S.H. Lee, Solid State Phenom. 118 (2006) 35–40.